International Journal of Nanomedicine

Dovepress
open access to scientific and medical research

Open Access Full Text Article

ORIGINAL RESEARCH

Novel silk fibroin nanoparticles incorporated silk fibroin hydrogel for inhibition of cancer stem cells and tumor growth

This article was published in the following Dove Press journal:
International Journal of Nanomedicine

Puyuan Wu
Qin Liu
Qin Wang
Hanqing Qian
Lixia Yu
Baorui Liu
Rutian Li

The Comprehensive Cancer Center of Drum Tower Hospital, Medical School of Nanjing University, Clinical Cancer Institute of Nanjing University, Nanjing, People's Republic of China

Background: A multi-drug delivery platform is needed as the intra-tumoral heterogeneity of cancer leads to different drug susceptibility. Cancer stem cells (CSCs), a small population of tumor cells responsible for tumor seeding and recurrence, are considered chemotherapy-resistant and have been reported to be sensitive to salinomycin (Sal) instead of paclitaxel (Ptx). Here we report a novel silk fibroin (SF) hydrogel-loading Sal and Ptx by incorporating drug-loaded silk fibroin nanoparticles (SF-NPs) to simultaneously kill CSCs and non-CSCs.

Methods: Using the method we have previously reported to prepare Ptx-loaded SF-NPs (Ptx-SF-NPs), Sal-loaded SF-NPs (Sal-SF-NPs) were fabricated under mild and non-toxic conditions. The drug-loaded SF-NPs were dispersed in the ultrasound processed SF solution prior to gelation.

Results: The resulting SF hydrogel (Sal-Ptx-NP-Gel) retained its injectable properties, exhibited bio-degradability and demonstrated homogeneous drug distribution compared to the non-NP incorporated hydrogel. Sal-Ptx-NP-Gel showed superior inhibition of tumor growth compared to single drug-loaded hydrogel and systemic dual drug administration in the murine hepatic carcinoma H22 subcutaneous tumor model. Sal-Ptx-NP-Gel also significantly reduced $CD44^{+}CD133^{+}$ tumor cells and demonstrated the least tumor formation in the in vivo tumor seeding experiment, indicating superior inhibition of cancer stem cells.

Conclusion: These results suggest that SF-NPs incorporated SF hydrogel is a promising drug delivery platform, and Sal-Ptx-NP-Gel could be a novel and powerful locoregional tumor treatment regimen in the future.

Keywords: silk fibroin, nanoparticle, hydrogel, salinomycin, cancer stem cells

Introduction

Hydrogel systems applied in cancer therapy are aimed to locoregionally eradicate tumors by local drug delivery with limited systemic toxicity.[1,2] However, tumor heterogeneity has been reported as one of the major obstacles in cancer therapy.[3–5] The intra-tumoral differences in the genetic and pathological backgrounds of cancer cells leads to differences in drug susceptibility.[4] More importantly, cancer stem cells (CSCs), that possess the capacity of self-reproduction, self-renewal and unlimited growth, are only a small fraction of tumor cells, but they are considered to be the root cause of tumor recurrence.[6,7] Unfortunately, studies have shown that CSCs are resistant to most anticancer drugs which were designed to kill non-CSC cancer cells.[8,9] Thus, dual- or multi-drug delivery platforms designed to target both CSCs and non-CSC cancer cells are desirable.

Salinomycin (Sal), an antibiotic potassium ionophore, has been demonstrated as an effective CSC-specific inhibitor.[10–12] Sal not only inhibited cancer cells of various cell

Correspondence: Rutian Li; Baorui Liu
The Comprehensive Cancer Center of Drum Tower Hospital, 321 Zhongshan Road, Nanjing 210008, People's Republic of China
Tel +86 25 8310 6666 ext 61341;
+86 25 8310 6666 ext 61331
Email li_rutian@163.com;
baoruiliu@nju.edu.cn

submit your manuscript | www.dovepress.com
Dovepress
http://dx.doi.org/10.2147/IJN.S166104

types with stem cell markers and the tumor sphere formation in vitro but also demonstrated anti-tumor efficacy in vivo. Sal inhibited CSCs by interfering with the Akt signaling pathway, Wnt/β-catenin, Hedgehog and Notch pathways.[12] Although clinical pilot studies have been conducted, Sal currently has a narrow therapeutic window as a commonly used veterinary antibiotic.[13] Sal poisoning is fatal and is without any effective antidote.[14] Therefore, we hypothesized that the locoregional and controlled delivery of Sal could be safer and more efficient.

Traditional chemotherapy has been reported to promote cancer stemness by chemotherapy-induced senescence.[15] Several studies have reported that paclitaxel (Ptx) enriched CSCs with the overexpression of CSC surface markers or CSCs associated pathways and low expression of EMT-associated E-cadherin.[10,16,17] Sal has shown notable activity against Ptx-resistant CSCs.[10] Furthermore, studies have shown that Sal sensitized antimitotic drug Ptx.[18–20] Thus, co-delivery of Sal and Ptx could be an effective local treatment.

The biocompatibility of hydrogels is as important as effectiveness for future clinical use.[1] Silk fibroin (SF) has been proved to be a biocompatible native biomolecule and has a safe record in vivo.[21,22] Although chemically cross-linked SF hydrogels have tunable elasticity and other mechanical properties,[23,24] ultrasound induced physically cross-linked SF hydrogels have the advantage of injectability as well as biocompatibility and safety without any toxic initiators or cross-linkers.[25,26] Additionally, SF hydrogel could be loaded with doxorubicin, and effectively inhibit primary breast cancer in a mouse model.[27] Although SF hydrogel containing SF NPs which is loaded with hydrophilic dyes has been reported,[28] the development of new strategies to load SF hydrogel with hydrophobic cancer therapeutic drugs, such as Sal and Ptx, are desired.

We have recently reported a novel and non-toxic method to prepare Ptx-loaded silk fibroin nanoparticles (Ptx-SF-NPs).[29,30] In this study, we successfully prepared Sal-loaded silk fibroin nanoparticles (Sal-SF-NPs) by using a similar method. We fabricated the silk fibroin hydrogel-loading hydrophobic drugs based on nanoparticle dispersion. The present investigation outlines the characterization of nanoparticles and hydrogels, and the toxicity, anti-tumor efficacy and inhibition of CSCs.

Materials and methods

Materials

Cocoons of *Bombyx mori* silkworm were procured from Jiangsu Province, China. Sal was provided by the China Institute of Veterinary Drugs Control (Beijing, China). Ptx was provided by the Jiangsu Yew Pharmaceutical Co., Ltd (Jiangsu, China). Ptx injection was provided by the Yangtze River Pharmaceutical Group (Jiangsu, China). Protease XIV (Sigma-Aldrich Co., St Louis, MO, USA), 2,4-dinitrophenylhydrazine (Sigma-Aldrich, USA), anti-human/mouse CD44 APC (eBioscience, Inc., San Diego, CA, USA), and anti-mouse CD133 PE (eBioscience Inc.) were used as received. Acetonitrile (EMD Millipore, Billerica, MA, USA) and methanol (EMD Millipore) were of HPLC grade. Milli-Q ultra-pure water was used. Anhydrous calcium chloride, absolute ethanol and other chemicals were of analytical grade and used without further purification. Murine hepatic carcinoma cell line H22 was purchased from the Shanghai Institute of Cell Biology (Shanghai, China).

Silk fibroin extraction and purification

The SF aqueous solution was prepared as previously reported.[29] Briefly, the cocoons were cut into small pieces and degummed for 30 minutes twice in boiled 0.5% sodium carbonate followed by thorough washing with deionized water. The degummed SF was dissolved in a ternary solution (molar ratio $CaCl_2/CH_3CH_2OH/H_2O$=1:2:8) at 70°C for 4 hours. The resulting solution was dialysed (molecular weight cut-off [MWCO] 14,000 Da) against ultra-pure water for 4 days to remove salts and ethanol. After centrifugation (10,000 rpm for 15 minutes) to spin down the debris and filtration through a 0.22-μm filter for sterilization, the SF aqueous solution (50 mg/mL) was stored at 4°C and diluted with sterilized Milli-Q water prior to use. The concentration of SF solution was determined by weighing the residual solid after drying at 50°C for 24 hours.

Sal-loaded silk fibroin nanoparticle preparation

Sal-SF-NPs were prepared in aqueous solution under ambient temperature. Sal dissolved in ethanol was introduced dropwise into 15 mg/mL SF solution under constant stirring. The resulting milky bluish solution was filtered and centrifuged at 12,000 rpm for 45 minutes. The pellets were washed twice and re-suspended in saline by using an ultrasound processor SONICS Vibra-cell VCX130 (Sonics & Materials, Inc., Newtown, CT, USA) at 20% amplitude for 2 seconds. Ptx-SF-NPs were prepared as previously reported.[29]

Nanoparticle characterization

Particle size and ζ potential

Sal-SF-NPs particle size and polydispersity (PDI) were measured in triplicate by dynamic light scattering (DLS)

with the Brookhaven BI-900AT instrument (Brookhaven Instruments Corporation, Holtsville, NY, USA) at 25°C. The ζ potential was determined in octuplet by a ζ potential analyzer (Brookhaven Instruments Corporation, USA).

Morphology study

The morphological study of Sal-SF-NPs was conducted under-JEM-1011 (Japan) transmission electron microscopy (TEM). Copper wire meshes were immersed in the Sal-SF-NP aqueous solution for seconds and air-dried prior to observation without staining.

Infrared spectra and X-ray diffraction

To investigate the conformation of SF in Sal-SF-NPs, infrared spectra were recorded with a Fourier transform infrared spectrophotometer (FTIR) (Bruker VERTEX 80V, Ettlingen, Germany). Lyophilized regenerated silk fibroin (LSF) and degummed silk fibroin fiber (SFF) were also examined. The spectra were all recorded at a resolution of 4 cm^{-1} and were generated from 64 scans. To determine the β-sheet structure and crystallinity of SF in Sal-SF-NPs, the X-ray diffraction (XRD) intensity curves were measured by a Rigaku Ultima III X-ray diffractometer (Rigaku Corporation, Tokyo, Japan). LSF and SFF were also examined. The curves were all recorded at a scanning rate of 3°/min with the scanning region of 3°–45°.

Drug loading content and encapsulation efficiency

The drug loading content and encapsulation efficiency of Sal-SF-NPs were analyzed by the Agilent HPLC system with a Zorbax C18 column (150×4.6 mm, 5 μm, Agilent Technologies, Santa Clara, CA, USA) by using a pre-column derivatization method.[31] Briefly, samples were dissolved in 700 μL of methanol and a volume of 200 μL of trichloroacetic acid aqueous solution was added to each sample. After adding 100 μL of 2,4-dinitrophenyl-hydrazine (DNP), the samples were incubated at 55°C for 30 minutes followed by HPLC. The mobile phase was methanol/1.5% aqueous acetic acid (90/10, v/v). The retention time for Sal was 16.3 minutes at 362 nm detection wavelength. The drug loading and encapsulation were assessed by HPLC for three independent batches of NPs. The drug loading content (DL) and encapsulation efficiency (EE) were calculated by the following equations:

$$DL\% = \frac{\text{Weight of the drug in NPs}}{\text{Weight of NPs}} \times 100\%$$

$$EE\% = \frac{\text{Weight of the drug in NPs}}{\text{Weight of the feeding drug}} \times 100\%.$$

Sal-Ptx-NP-Gel preparation

Ultrasound induced silk fibroin hydrogel was prepared as reported with mild modifications.[25] Briefly, 1 mL SF aqueous solution in a 1.5 mL Eppendorf tube was sonicated with an ultrasonic processor Sonics Vibra-Cell™ VCX 130 (Sonics & Materials, Inc.) at 60% amplitude for 1 minute. After the solution was cooled to room temperature within 3 minutes, Sal-SF-NPs and Ptx-SF-NPs were dispersed in the solution with the ultrasound processor at 20% amplitude for 2 seconds to prepare the Sal-Ptx-NP-Gel. For the injectable hydrogel formulation and drug loading homogeneity study, the sonicated solution was aspirated into a 1 mL syringe and incubated vertically at 60°C for 1 hour to ensure the sol-gel transition. For the swelling study, in vitro degradation study and in vitro drug release studies, 500 μL of the sonicated solution was pipetted onto a Millicell insert (Millipore PCF 3 μm) and incubated for gel formation. For Sal-Ptx-non-NP-Gel, powder of pristine Sal and Ptx, instead of drug-loaded SF NPs, was dispersed in the sonicated solution at 30% amplitude for 5 seconds.

Hydrogel characterization

Infrared spectra and X-ray diffraction

To investigate the conformation of SF in the Ptx-Sal-NP-Gel, spectra of FTIR and XRD were recorded with the same parameter settings as reported above. Lyophilized blank SF hydrogel (Gel) and Ptx-Sal-non-NP-Gel were also examined.

Swelling study

To study the swelling property of SF hydrogel, hydrogels in Millicell inserts were incubated in 4 mL of 0.01 M PBS, pH 7.4, at 37°C. At predetermined time points, the inserts were collected and blotted to remove excess water on the gel surface, and subsequently weighed. The swelling ratio (SR) was calculated by the following equation:

$$SR = \frac{\text{Gel weight}}{\text{Initial gel weight}}.$$

In vitro degradation study

To study the in vitro degradation of SF hydrogel, hydrogel in Millicell inserts was incubated in 4 mL of Protease XIV solution (2.5 units per 5 mg SF) at 37°C. The control hydrogel was placed in 4 mL of PBS. The solutions were replaced every 4 days. At the indicated times, the inserts were collected and photographed.

Drug-loading homogeneity study

To determine the drug-loading homogeneity of nanoparticles incorporated hydrogel, Sal-Ptx-NP-Gel and Sal-Ptx-non-NP-Gel were prepared in 1 mL syringes, which were vertically placed during the sol-gel transition so that the insoluble drug particles aggregated and gathered in the lower region of the syringe. A volume of 0.2 mL of hydrogel was successively injected from the syringe to obtain five samples from different parts of the syringes, labelled part 1, 2, 3, 4 and 5 of the hydrogel. The samples were dried, followed by drug content determination using HPLC. Sal was quantified as described above in 'Drug loading content and encapsulation efficiency'. For Ptx quantification, the mobile phase was acetonitrile/water (52/48, v/v). The retention time for PTX was 5.5 minutes at a 227 nm detection wavelength. The relative drug content (RDC) of each part of the hydrogel was calculated by the following equation:

$$RDC = \frac{\text{Drug weight}}{\text{Average drug weight of the five parts}}$$

Average drug weight was calculated as the average of all of the five samples. The drug loading homogeneity was assessed by three independent batches of Sal-Ptx-NP-Gel and Sal-Ptx-non-NP-Gel.

In vitro drug release study

To determine the drug release pattern from SF hydrogel, Ptx-NP-Gel and Sal-NP-Gel were prepared in Millicell inserts. For Ptx release, the inserts were placed in 8 mL of PBS buffer with 0.5% Tween80. For Sal release, the inserts were immersed into 4 mL PBS. Release buffers were replaced at indicated times. The drug content in the release buffer was determined by HPLC as described above.

In vivo toxicity study of Sal-Ptx-NP-Gel

The animal experiments were approved by the Animal Care Committee at Drum Tower Hospital, Nanjing, China. Healthy drug naïve male ICR mice with body weight of 25±2 g were raised under a specific pathogen-free (SPF) environment in compliance with the guidelines set by the committee. For the in vivo toxicity study, the mice were randomly divided into six groups; and each group contained three mice. On day 1, six groups of mice were treated with Sal solution (2 mg/kg, intraperitoneal injection [IP]), Sal solution (4 mg/kg, IP), Sal solution (2 mg/kg, subcutaneous injection [IH]), Sal solution (4 mg/kg, IH), Sal-Ptx-NP-Gel (2 mg/kg Sal, IH) and Sal-Ptx-NP-Gel (4 mg/kg Sal, IH), respectively. Survival were observed. On days 7, 14 and 28, the mice in the group treated with Sal-Ptx-NP-Gel (4 mg/kg Sal, IH) were sacrificed. Heart, liver, and skeletal muscle samples were collected for H&E staining.

In vivo tumor and cancer stem cells inhibition study

In vivo antitumor efficacy

The animal experiments were approved by the Animal Care Committee at Drum Tower Hospital, Nanjing, China. To investigate the in vivo anti-tumor efficacy of Sal-Ptx-NP-Gel, a subcutaneous murine hepatic cancer H22 tumor-bearing mouse model was used. Healthy drug naïve male ICR mice weighing of 20±2 g were raised under an SPF environment in compliance with the guidelines set by the committee. A volume of 0.2 mL of saline containing 2×10^6 H22 cells was subcutaneously injected into the lower right axilla of the mice. When the tumors reached 100–300 mm^3 in volume, the mice were randomly divided into eight groups with each group comprising six mice. The day was marked as "Day 1". On day 1, eight groups were treated with normal saline (NS), blank SF gel, Ptx injection (18 mg/kg Ptx, intravenous injection [IV]), Sal solution (2 mg/kg/d Sal, IP, day 1 and 2), Ptx injection with Sal solution (18 mg/kg Ptx, IV; 2 mg/kg/d Sal, IP, day 1 and 2), Ptx-NP-Gel (18 mg/kg Ptx, peritumoral injection [PT]), Sal-NP-Gel (4 mg/kg Sal, PT) and Sal-Ptx-NP-Gel (18 mg/kg Ptx and 4 mg/kg Sal PT), respectively. Tumor sizes were measured daily by Vernier calipers, and the tumor volumes were calculated as $V=D\times d^2/2$ (D and d were the longest and the shortest diameter of tumor in mm, respectively). Relative tumor volumes were calculated by the following equation to reduce the impact of initial tumor volume differences after grouping:

$$\text{Relative tumor volume} = \frac{V}{V_0}$$

where: V was the absolute tumor volume, and V_0 was the average tumor volume of the group on Day 1. On day 7, the mice were sacrificed. Tumors were collected for pathological study by H&E staining.

Flow cytometry of cancer stem cells

Each tumor from groups treated with saline, Ptx-NP-Gel, Sal-NP-Gel and Sal-Ptx-NP-Gel was minced, filtered through a 200-mesh sieve, washed with saline and re-suspended in saline to make single cell suspensions for further experiments. The ratio of $CD44^+CD133^+$ cancer stem cells in the single cell suspensions was investigated by a flow cytometry (BD FACS Aria II, BD Biosciences, San Jose, CA, USA). The randomly

selected three samples from each group were incubated with anti-human/mouse CD44 allophycocyanin and anti-mouse CD133 PE for 15 minutes at the manufacturer's recommended concentration. After washing twice with saline, the cell suspensions were analyzed by flow cytometry.

Tumor seeding study

To investigate the tumor seeding ability of the tumors after treatment, the single cell suspensions were re-injected into healthy male ICR mice to monitor tumor formation. In each group, three samples of the single cell suspensions were mixed and counted for cell concentration. A volume of 0.2 mL of saline containing 10^6, 10^4 or 10^3 cells was subcutaneously injected into lower right axilla of the mice. Tumor incidence was monitored for 45 days after injection, and tumor formation was assayed by palpation. In the group of 10^6 cells, tumor sizes were measured and survival was monitored.

Statistical analysis

The data are listed as the means ± SD except the DLS, ζ potential and animal experiments, where data are listed as the means ± SEM. Statistical analysis of the data was made by ANOVA, Student's *t*-test or the Mann–Whitney U test. $P<0.05$ was considered significantly different.

Results

Fabrication and characterization of Sal-loaded silk fibroin NPs

Sal-SF-NPs were fabricated by using a method similar to that used to prepare Ptx-SF-NPs. The SF aqueous solution turned milky after introducing Sal ethanol solution (Figure 1A, right), while no obvious change was observed by adding an equivalent volume of ethanol without Sal (Figure 1A, left). The self-assembling Sal-SF-NPs were round shaped under TEM with a dense core and a thin

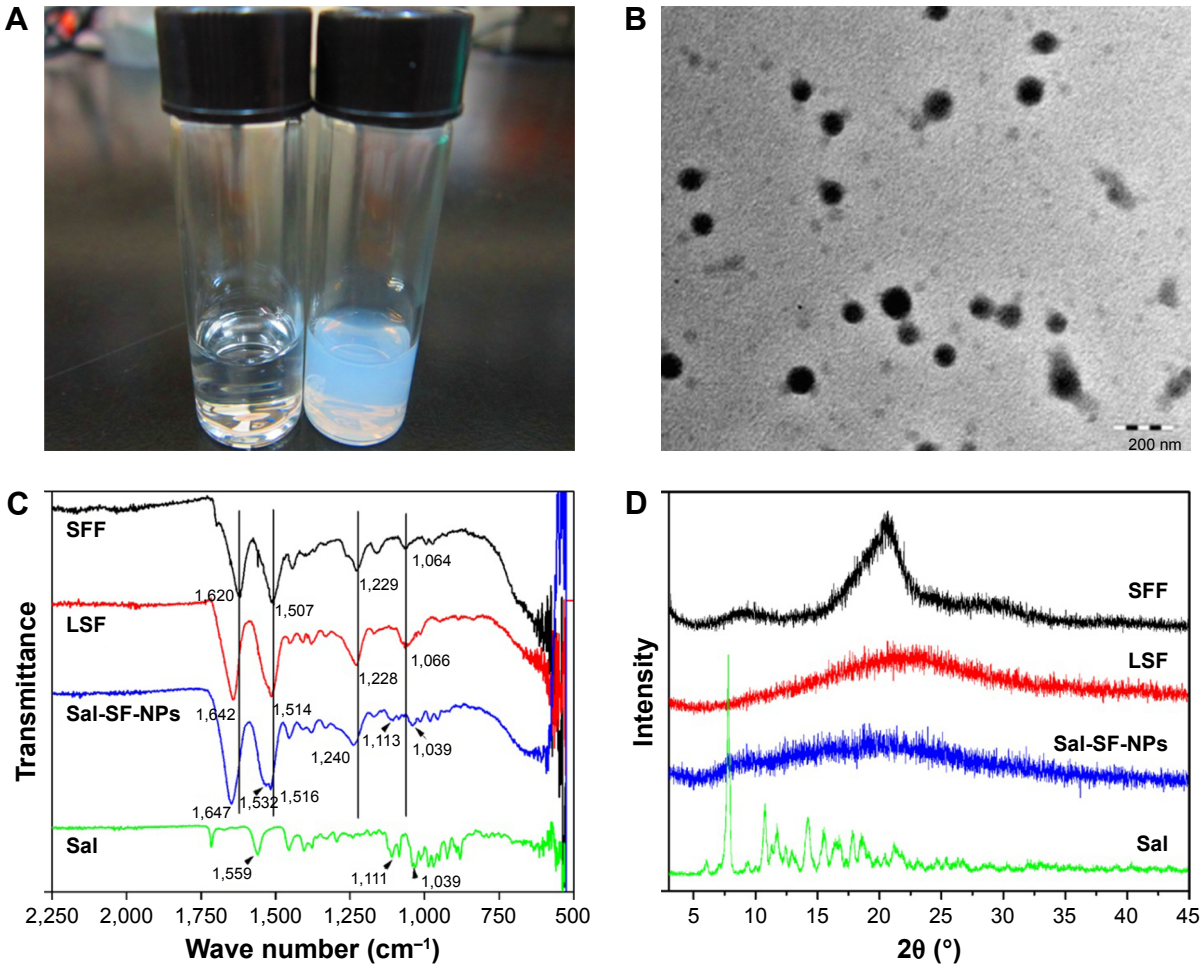

Figure 1 Fabrication and characterization of Sal-SF-NPs.

Notes: (**A**) The formation of Sal-SF-NPs. Right, SF solution adding Sal ethanol solution. Left, SF solution adding equivalent ethanol. (**B**) TEM of Sal-SF-NPs. (**C**) FTIR of Sal-SF-NPs. (**D**) XRD of Sal-SF-NPs. SFF and LSF were recorded as controls for silk II and silk I conformation, respectively.

Abbreviations: Sal, salinomycin; SF, silk fibroin; NPs, nanoparticles; FTIR, Fourier transform infrared spectroscopy; TEM, transmission electron microscopy; XRD, X-ray diffraction; SFF, silk fibroin fiber; LSF, lyophilized regenerated silk fibroin.

Table 1 Characterization of Sal-SF-NPs fabricated by different silk concentrations and drug feedings

SF (mg/mL)	Sal (mg)	Dh (nm)	PDI	ζ potential (mV)
10	6	271.1±1.6	0.141±0.019	−32.39±4.15
15	6	241.0±2.1	0.147±0.036	−14.24±2.61
15	9	239.2±4.4	0.148±0.020	−14.65±2.63

Abbreviations: Sal, salinomycin; SF, silk fibroin; NPs, nanoparticles; Dh, hydrodynamic diameter; PDI, polydispersity index.

corona (Figure 1B). The average diameter of Sal-SF-NPs under TEM was approximately 120 nm (Figure 1B). The DLS hydrodynamic diameter and ζ potential varied with SF concentration instead of drug feeding (Table 1). The SF concentration of 15 mg/mL and Sal feeding of 6 mg were selected for the next experiment. The drug loading and encapsulation efficiency of Sal-SF-NPs were 12.1%±2.3% and 34.7%±1.0%, respectively.

To investigate the conformation of SF in Sal-SF-NPs, FTIR spectra (Figure 1C) and XRD (Figure 1D) were recorded. In IR spectra, SFF with a typical silk II structure comprising β-sheets had characteristic absorption bands at 1,620 (amide I), 1,507 (amide II), 1,229 (amide III), and 1,064 cm^{-1} (amide IV). LSF with mainly silk I structure composed of α-helices and random coils had absorption frequencies at 1,642 (amide I), 1,514 (amide II), 1,228 (amide III), and 1,066 cm^{-1} (amide IV). Sal-SF-NPs had absorption at 1,647 (amide I), 1,516 (amide II) and 1,240 cm^{-1} (amide III), which were shifted from β-sheets structure, indicating a silk I or random coil conformation. Additional peaks at 1,113 and 1,039 cm^{-1} instead of amide IV in Sal-SF-NPs were characteristic of Sal encapsulated in NPs, confirmed by pristine Sal IR spectrum. In XRD, the characteristic diffraction peaks of β-sheets crystalline at 2θ=20.19° were observed in SFF. For LSF and Sal-SF-NPs, no obvious peak was detected at 2θ=20.19°, which was consistent with IR results showing that random coils instead of β-sheets were the conformation of SF in Sal-SF-NPs. The intensive peaks of pristine Sal were not obvious in Sal-SF-NPs, which proved that Sal was encapsulated in the NPs in an amorphous state.

Preparation and characterization of Sal-Ptx-NP-Gel

Ultrasound-induced SF hydrogel was fabricated by sonicating SF aqueous solution and incubating the sonication processed SF solution (Figure 2A, right) at 60°C for 1 hour. After dispersing the drug-loaded SF-NPs in the sonication-processed solution (Figure 2A, middle) followed by incubation, Sal-Ptx-NP-Gel was prepared (Figure 2A, left). Sal-Ptx-NP-Gel could be injected through a 26G needle from a prefilled syringe (Figure 2B), indicating this gel as a potential minimally invasive treatment. SF hydrogel showed no swelling during a 10-days' observation (Figure 2C). In vitro degradation study demonstrated that SF hydrogel was biodegradable. While SF hydrogel showed no obvious change in PBS for 21 days, SF hydrogel in protease solution gradually turned transparent with reduced volume (Figure 2D). Incorporating SF-NPs did not change the stability of the hydrogel in PBS as indicated by the drug release study.

In IR spectra (Figure 3A), blank SF hydrogel (Gel) had characteristic absorption bands at 1,619 (amide I), 1,514 (amide II), 1,233 (amide III), and 1,063 cm^{-1} (amide IV), while Sal-Ptx-NP-Gel had absorption frequencies at 1,619 (amide I), 1,514 (amide II), 1,230 (amide III), and 1,066 cm^{-1} (amide IV). The wavenumber of amide I indicated the β-sheet conformation in Gel and Sal-Ptx-NP-Gel. In the XRD spectrum (Figure 3B), both Gel and Sal-Ptx-NP-Gel had the characteristic diffraction peaks of crystalline β-sheets at 2θ=20.19°. Thus, during the sol-gel transition, SF conformation was transformed from α-helices and random coils to the β-sheets structure.

Drug-loading homogeneity and release pattern

To prove the drug-loading homogeneity of nanoparticle incorporated hydrogel, both drug loading Sal-Ptx-NP-Gel and Sal-Ptx-non-NP-Gel were prepared in 1 mL syringes, which were vertically placed during the sol-gel transition so that the insoluble drug particles aggregated and gathered in the lower part of the syringes (Figure 2E). A volume of 0.2 mL of hydrogel was successively injected out of the syringe to obtain five samples from the different parts of the syringes (Figure 2E). In NP-Gel, there was no significant difference ($P>0.05$) in the relative drug contents for both Ptx and Sal (Figure 2F), indicating the homogeneity of drug distribution. However, in non-NP-Gel, there was a significant difference ($P<0.05$) in relative drug contents for both Ptx and Sal (Figure 2F). In addition, the differences of IR and XRD of Sal-Ptx-NP-Gel and Sal-Ptx-non-NP-Gel (Figure 3A and B) demonstrated that the hydrophobic Ptx and Sal were encapsulated in Sal-Ptx-NP-Gel in an amorphous state, which explained the homogeneous drug distribution.

We next investigated the in vitro drug release pattern from SF hydrogel. Ptx was continuously released from the hydrogel for more than 30 days (Figure 3C). The releasing

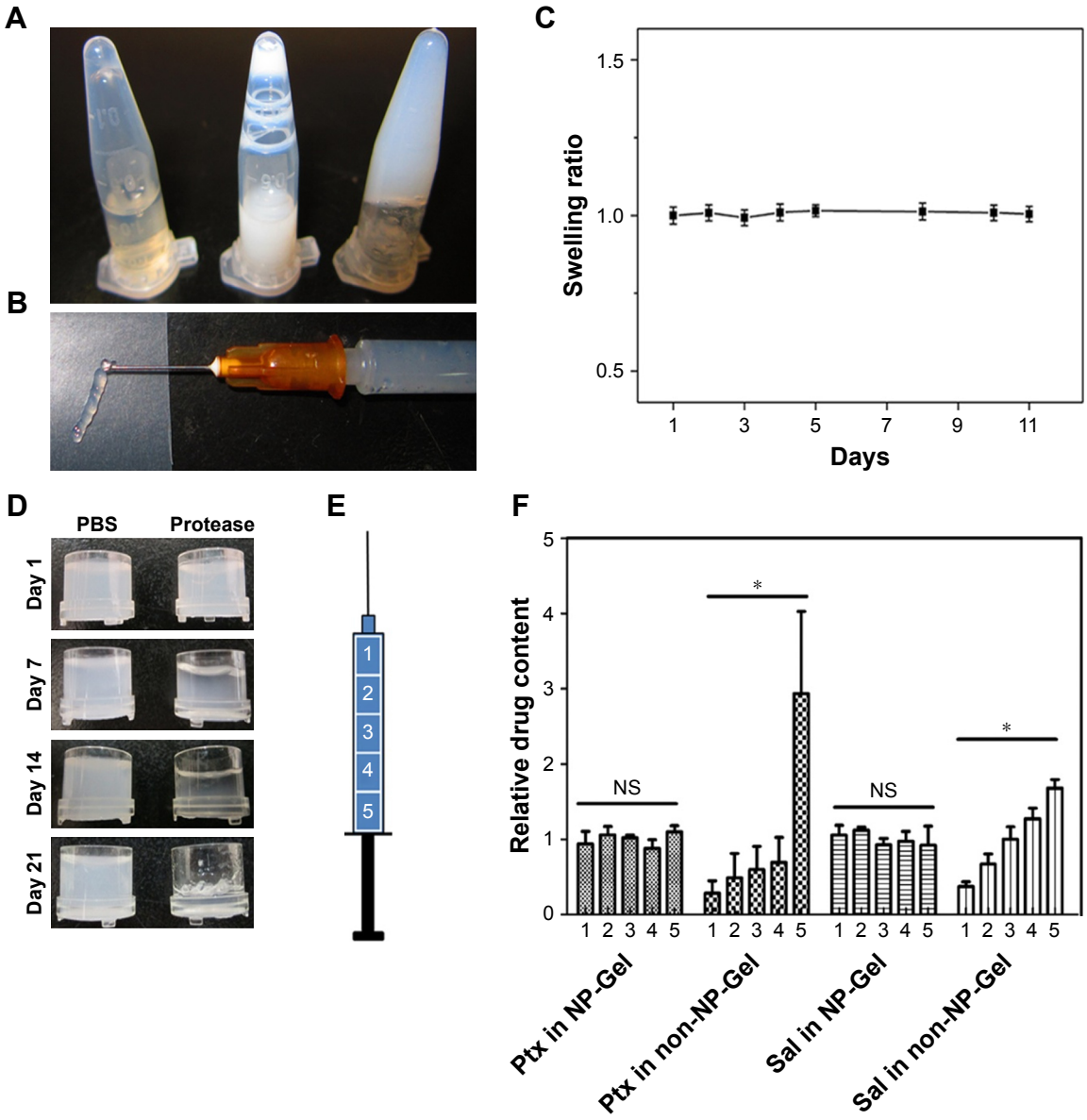

Figure 2 Preparation and characterization of Sal-Ptx-NP-Gel.
Notes: (**A**) Preparation of Sal-Ptx-NP-Gel. Left, sonicated SF solution; Middle, Sal-SF-NPs and Ptx-SF-NPs dispersed in sonicated SF solution; right, formation of Sal-Ptx-NP-Gel. (**B**) Injectable Sal-Ptx-NP-Gel from a 26G syringe needle. (**C**) Swelling ratio of SF hydrogel as a function of time. (**D**) In vitro degradation of SF hydrogel. (**E**) Schematic plot of drug loading homogeneity study. Syringes containing SF solution were vertically placed during sol-gel transition. Drug contents of five different parts of the hydrogel were determined by HPLC. (**F**) Relative drug content of five parts in NP-Gel and non-NP-Gel. *$P<0.05$.
Abbreviations: NS, no significance; Sal, salinomycin; Gel, hydrogel; Ptx, paclitaxel; SF, silk fibroin; NP, nanoparticle.

rate was faster in the first 10 days and remained steady in the next 20 days. On day 30, there was significant difference ($P<0.05$) in the cumulative drug release for different concentrations of SF, indicating that the higher the concentration of SF in the hydrogel the slower the drug release rate. Sal, another hydrophobic drug, showed a different release pattern compared with Ptx (Figure 3D). A burst release was observed and 83.8%±1.7% of Sal was released in the first 9 hours. Subsequently, 94.5%±1.7% of salinomycin was released in 24 hours and 98.3%±0.3% in 5 days. Thus, the drug release pattern of SF hydrogel was mainly dependent on the SF concentration and physicochemical property of the drug.

In vivo toxicity study

The toxicity study showed that Sal-Ptx-NP-Gel increased the maximum tolerated dose of Sal. ICR mice all survived after subcutaneous injection of Sal-Ptx-NP-Gel containing 4 mg/kg Sal above the lethal dose of 2 mg/kg pristine Sal (Table 2). Sal-Ptx-NP-Gel with 4 mg/kg Sal was well

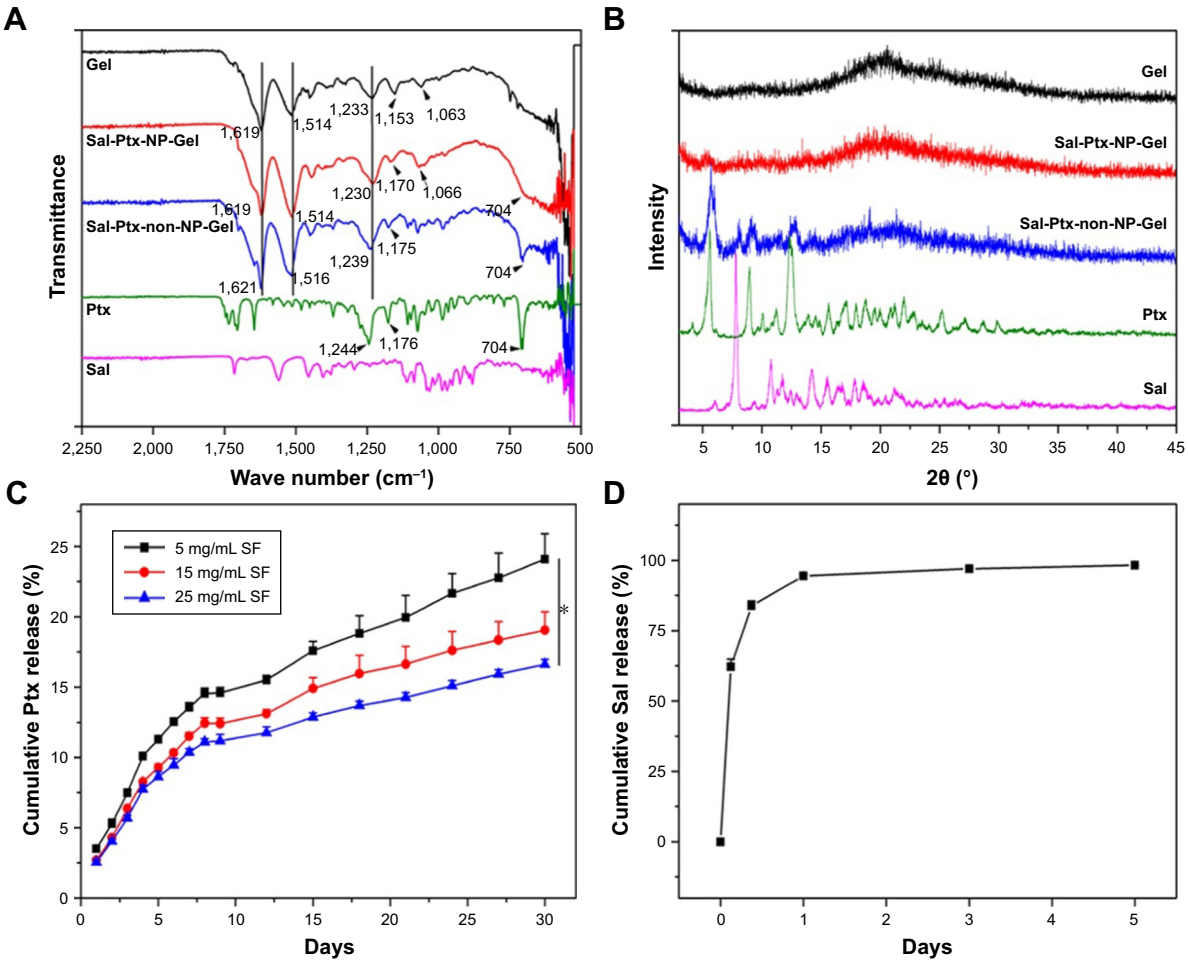

Figure 3 Characterization of Sal-Ptx-NP-Gel.
Notes: (**A**) FTIR of Sal-Ptx-NP-Gel. (**B**) XRD of Sal-Ptx-NP-Gel. (**C**) In vitro Ptx release from SF hydrogel as a function of time. *$P<0.05$. (**D**) In vitro Sal release from SF hydrogel as a function of time.
Abbreviations: FTIR, Fourier transform infrared spectroscopy; Sal, salinomycin; Ptx, paclitaxel; Gel, hydrogel; SF, silk fibroin; NP, nanoparticle; XRD, X-ray diffraction.

tolerated, and there was no obvious change in H&E staining of the heart, liver, and skeletal muscles (Figure 4), indicating the in vivo safety of Sal-Ptx-SF-NPs.

In vivo anti-tumor efficacy of Sal-Ptx-NP-Gel

The anti-tumor efficacy of Sal-Ptx-NP-Gel was evaluated on a subcutaneous H22 tumor-bearing ICR mouse model, and the experimental groups included single drug and combination drug regimens by systemic and locoregional administrations (Figure 5A). The combined administration of Ptx injection and Sal solution demonstrated significantly smaller relative tumor size (4.98±0.51) than the single injection of the drug Ptx injection (7.52±0.53) or Sal solution (7.26±0.51) ($P<0.05$) (Figure 6B). The locoregional administration of Sal-Ptx-NP-Gel showed the smallest tumor size (2.32±0.30), and there was a significant difference ($P<0.05$) between Sal-Ptx-NP-Gel administration and systemic drug administration (Figure 5B). In addition, hydrogel loading a single drug also exhibited better local tumor control than systemic single drug treatment (Figure 5C and D), although these treatments were not as effective as the combination drug delivery of the hydrogel Sal-Ptx-NP-Gel. Furthermore, pathological studies of the tumors were conducted as supplements of the tumor

Table 2 Survival of mice after Sal treatment in solution and Gel formation

Sal dosage (mg/kg)	Solution (IP)	Solution (IH)	Gel (IH)
2	3/3	3/3	3/3
4	0/3	0/3	3/3

Abbreviations: Gel, hydrogel; Sal, salinomycin; IP, intraperitoneal injection; IH, subcutaneous injection.

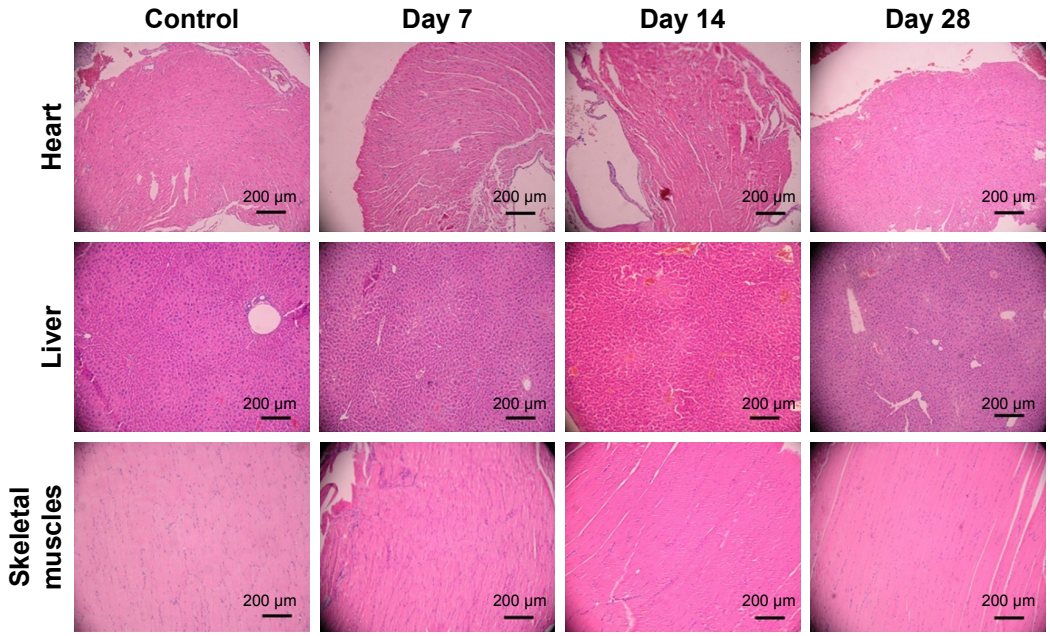

Figure 4 H&E staining of murine organs after the injection of Sal-Ptx-NP-Gel.
Abbreviations: Sal, salinomycin; Ptx, paclitaxel; NP, nanoparticle; Gel, hydrogel.

size study (Figure 5E). Necrotic areas were the most obvious in the Sal-Ptx-NP-Gel group, which explained the smallest tumor volumes at the pathological level.

In vivo cancer stem cell inhibition of Sal-Ptx-NP-Gel

To investigate the cancer stem cell inhibition of Sal-Ptx-NP-Gel, $CD44^+CD133^+$ cell ratios and tumor seeding abilities of group control, Ptx-NP-Gel, Sal-NP-Gel and Sal-Ptx-NP-Gel were evaluated. CD44 and CD133 have been reported as the surface markers of cancer stem cells, including hepatocarcinoma.[32] $CD44^+CD133^+$ double-positive cells were detected by flow cytometry, and the positive incidence was lower than 1% (Figure 6A–D). The $CD44^+CD133^+$ cell ratio of the Sal-Ptx-NP-Gel group (0.23%±0.03%) was significantly lower than that of the control group (0.44%±0.05%) ($P<0.05$), while there was no decline in the cancer stem cell ratios in the other two experimental groups (Figure 6E). Thus, Sal-Ptx-NP-Gel treatment decreased the proportion of $CD44^+CD133^+$ cancer stem cells.

Cancer stem cell inhibition of Sal-Ptx-NP-Gel was also assessed by a tumor seeding experiment. The results showed that Sal-Ptx-NP-Gel treatment resulted in a 10-fold decrease in tumor-seeding ability relative to the control group (Figure 6F). Furthermore, Sal-Ptx-NP-Gel group demonstrated slower tumor growth compared to any other groups when seeded with 10^6 cells ($P<0.05$) (Figure 6G) and the longest survival (Figure 6H). These findings indicated that Sal-Ptx-NP-Gel treatment decreased the tumor seeding ability of tumor cells.

Discussion

The use of hydrogel for clinical application is considered safe, biocompatible and effective. In the present study, we developed a dual drug delivery platform which was an SF hydrogel system loaded with Sal-SF-NPs and Ptx-SF-NPs for both CSCs and non-CSCs treatment. The characterization of drug-loaded SF-NPs, hydrogel swelling, in vitro degradability, drug-loading homogeneity, drug release pattern, in vivo toxicity, in vivo anti-tumor efficacy and in vivo CSC inhibition were comprehensively investigated. The Sal-Ptx-NP-Gel exhibited superior local tumor control effect and CSC inhibition efficacy.

SF is a natural bio-macromolecule widely studied as a tissue engineering material because of its excellent biocompatibility. Studies have reported that SF solution spontaneously undergoes a sol-gel transition over a long time.[33,34] To control the gelation kinetics or modify physical properties, various methods to prepare SF hydrogel have been reported.[23,24,35–38] In the present study, sonication-induced hydrogel exhibits no swelling, and is degradable and free of toxic cross-linkers, initiators or any other chemicals. Furthermore, consistent with other studies,[26,27,39] the hydrogel has been demonstrated as thixotropic and injectable, facilitating

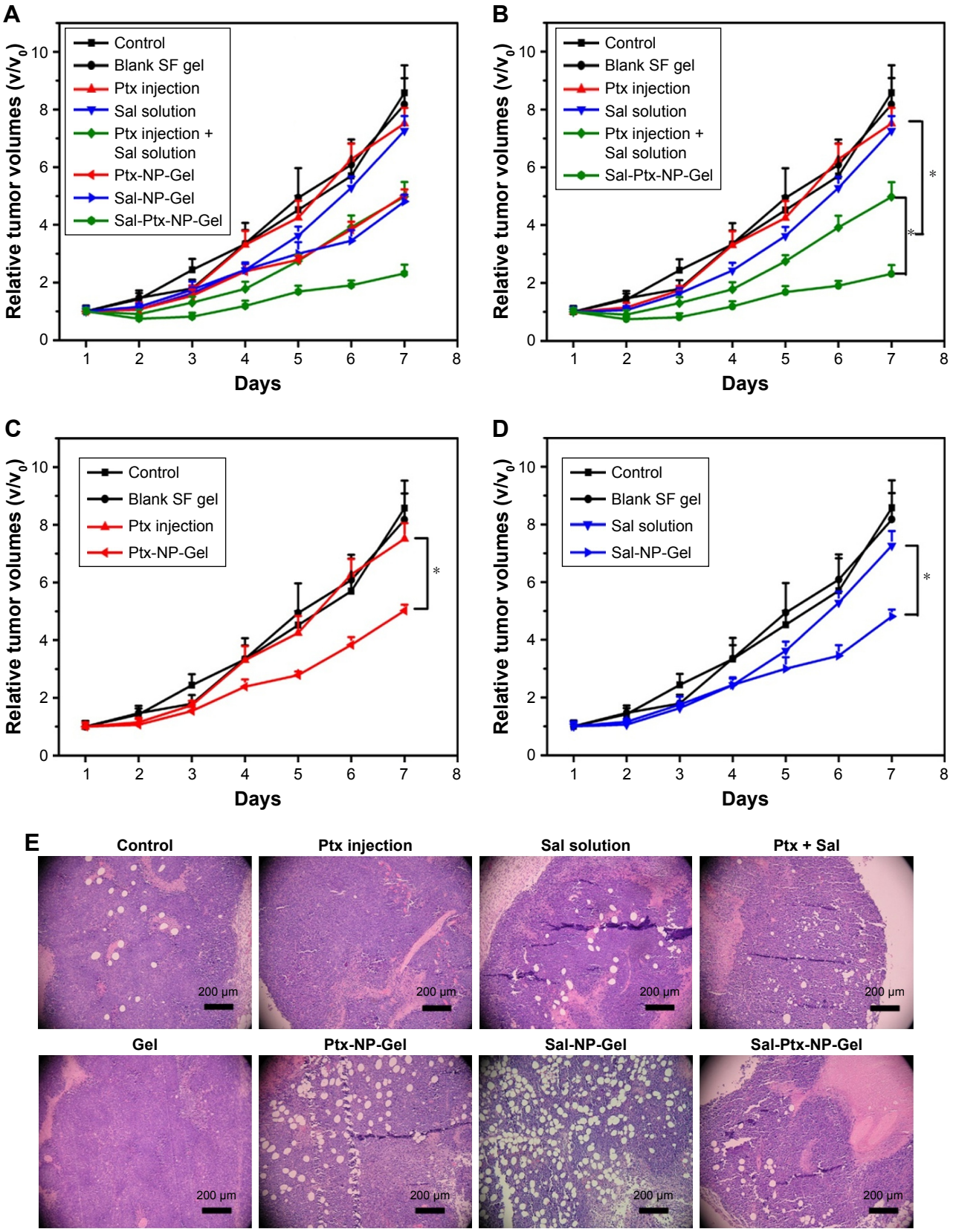

Figure 5 Anti-tumor efficacy of Sal-Ptx-NP-Gel.
Notes: (**A**) Relative tumor volumes after treatment. (**B**), (**C**) and (**D**) are parts of (**A**) to clearly demonstrate the results. *$P<0.05$. (**E**) H&E staining of the tumors.
Abbreviations: Sal, salinomycin; Ptx, paclitaxel; NP, nanoparticle; Gel, hydrogel.

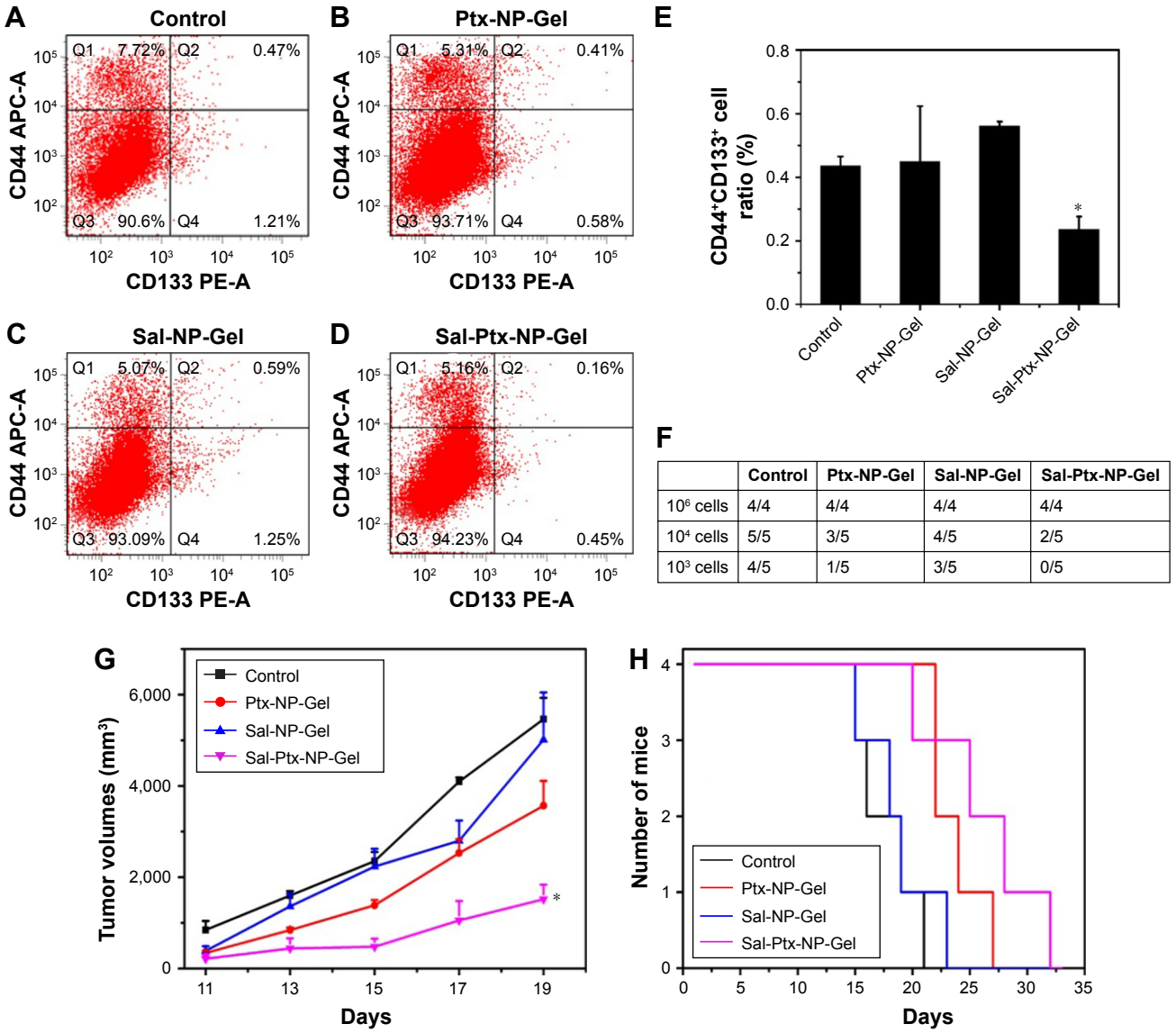

	Control	Ptx-NP-Gel	Sal-NP-Gel	Sal-Ptx-NP-Gel
10^6 cells	4/4	4/4	4/4	4/4
10^4 cells	5/5	3/5	4/5	2/5
10^3 cells	4/5	1/5	3/5	0/5

Figure 6 Cancer stem cell inhibition of Sal-Ptx-NP-Gel.
Notes: (**A**), (**B**), (**C**) and (**D**) Flow cytometry detection of $CD44^+CD133^+$ cancer stem cells in control, Ptx-NP-Gel, Sal-NP-Gel and Sal-Ptx-NP-Gel groups. (**E**) $CD44^+CD133^+$ cell ratios in each group. *$P<0.05$ compared with control group. (**F**) Tumor formation in tumor seeding experiments after primary treatment. (**G**) Tumor volumes of each group seeded with 10^6 tumor cells. (**H**) Survivals of each group seeded with 10^6 tumor cells.
Abbreviations: Sal, salinomycin; Ptx, paclitaxel; NP, nanoparticle; Gel, hydrogel.

local delivery by minimal invasive operation, which is clinically in demand.

SF hydrogels and nanoparticles have been reported for loading anticancer drugs, including doxorubicin,[27,38,40] vincristine,[39] cisplatin,[41] and 5-fluorouracil.[42] However, as a drug depot, which contains a large proportion of water, it was a challenge to load hydrophobic drugs into the SF hydrogel. Directly mixing the SF matrix with hydrophobic drugs, such as curcumin, has been used,[43,44] but this strategy might lead to drug-loading heterogeneity in SF hydrogel preparation, as confirmed in the present study. The precipitates of Ptx formed immediately after adding Ptx ethanol solution to SF aqueous solution. Although sonication was used before hydrogel formation in order to form a homogeneous system, the precipitates aggregated during the gelling time and caused heterogeneity of drug concentration. To solve this problem, we developed SF-NPs incorporated SF hydrogel based on a previous study of hydrophobic drug-loading SF-NPs. The resulting Sal-Ptx-SF-Gel exhibited drug-loading homogeneity and was suitable for further experiments. We believe that this dual or multi drug-loading platform could be used to load different drugs for various applications.

The secondary structural change of SF is important for understanding the inter- or intra-molecular force of SF protein. The molecular structure of SF consists of large regions of hydrophobic amino acids (repeated sequences of [Gly−Ala−Gly−Ala−Gly−Ser]n), separated by short hydrophilic regions. The present study demonstrated that SF could encapsulate hydrophobic Sal and self-assemble into nanoparticles with an α-helix or random coil conformation. We also observed the α-helix or random coil structure of Ptx-SF-NPs in a previous study. These results indicated that Sal-SF-NPs and Ptx-SF-NPs have a similar structure and SF could assemble into Silk-I rich nanoparticles when loaded with hydrophobic drugs. Instead of β-sheet formation between the repetitive sequences of the SF molecules, the nanoparticles with dense cores were formed by hydrophobic force between the drug and the repetitive hydrophobic sequences.

Previous studies have reported that the slow and sustained controlled release of the encapsulated doxorubicin from the SF hydrogels depended on the SF concentration.[27] In the present study, a similar release pattern was observed in the Ptx release experiment. However, another hydrophobic drug, Sal, was released with an obvious initial burst release, which was a pattern reported in antibodies released from SF hydrogel.[45,46] The differences in release were due to the drug property and drug-silk interaction. Although Sal was released faster than Ptx in vitro, SF hydrogel effectively increased the maximum tolerated dose of Sal in vivo. Furthermore, Sal-Ptx-NP-Gel was well tolerated in vivo with low toxicity. Based on the successful toxicity studies, in vivo antitumor studies were performed.

Sal preferentially inhibited cancer stem cells. Previous studies have shown that Sal is at least 100 times more effective than the anti-cancer drug Ptx in killing CSCs.[10] In vivo studies demonstrated a comparable inhibition rate between Sal and Ptx, which indicated that the strategy to kill only CSCs was not sufficient for tumor eradication. Thus, strategies to kill both CSCs and non-CSC cancer cells are needed. In the present study, the hydrophobic Sal was encapsulated in SF-NPs and subsequently incorporated into SF hydrogel with Ptx-SF-NPs. We found that combination of Sal and Ptx synergistically enhanced the anti-tumor efficacy, consistent with other studies.[15] Sal-Ptx-NP-Gel also decreased $CD44^{+}CD133^{+}$ cancer stem cell proportion and tumor seeding ability. However, we found that Sal-NP-Gel did not exhibit apparent CSC inhibition at the endpoint of the in vivo experiment. A single dose with relative rapid drug releasing of Sal might be the reason, since it is conceivable that non-CSCs within tumors can give rise to CSCs at a low but significant rate.[10,47] The Sal-Ptx-NP-Gel, which released Ptx in a sustained manner, inhibited non-CSCs and maintained the low ratio of CSCs.

The drug delivery platform presented here is proposed to include: 1) a multidrug delivery silk fibroin hydrogel loaded with multiple hydrophobic drugs; 2) a biosafety and biocompatible minimal invasive treatment; and 3) a hydrogel system designed based on tumor homogeneity, as advantages that synergistically inhibit tumor growth through Ptx killing non-CSC cells and Sal killing CSCs. Although the drug distribution and drug penetration of the hydrogel system should be further studied, the present study confirmed SF-NPs incorporated SF hydrogel as an effective drug carrier for Ptx and Sal and its enhanced antitumor efficacy by locoregional drug delivery.

Conclusion

Biocompatible Sal-Ptx-NP-Gel was fabricated without toxic organic solvents and surfactants. The hydrogel showed no swelling, in vitro degradability, drug-loading homogeneity and injectable properties. The drug release pattern primarily depended on the SF concentration and physicochemical property of the drug with sustained Ptx release and relatively rapid Sal release. Sal-Ptx-NP-Gel also increased the maximum tolerated dose of Sal. Furthermore, Sal-Ptx-NP-Gel showed superior anti-tumor efficacy for locoregional tumor treatment and CSC inhibition in vivo. The present study highlighted Sal-Ptx-NP-Gel as a biocompatible multi-drug delivery platform for locoregional chemotherapy, and its potential for further clinical application.

Acknowledgments

The work was supported by The National Key Research and Development Program of China (No 2017YFC1308900), National Natural Science Foundation of China (Nos 81602077, 81672398, 81672367, 81572601, 81472216), Program of Jiangsu Provincial Key Medical Center (No YXZXB2016002), Scientific and Technological Development Program of Nanjing (No 201605012), Natural Science Foundation of Jiangsu Province (Grant no BK20151095) and Nanjing Medical Youth Talent Training Project (No QRX17038). The abstract for the present study was presented at the 2015 ASCO Annual Meeting and published online (see https://meetinglibrary.asco.org/record/109244/abstract).

Disclosure

The authors report no conflicts of interest in this work.

References

1. Merino S, Martín C, Kostarelos K, Prato M, Vázquez E. Nanocomposite hydrogels: 3D polymer-nanoparticle synergies for on-demand drug delivery. *ACS Nano*. 2015;9(5):4686–4697.

2. Sepantafar M, Maheronnaghsh R, Mohammadi H, et al. Engineered hydrogels in cancer therapy and diagnosis. *Trends Biotechnol*. 2017;35(11):1074–1087.
3. Marusyk A, Almendro V, Polyak K. Intra-tumour heterogeneity: a looking glass for cancer? *Nat Rev Cancer*. 2012;12(5):323–334.
4. Senft D, Leiserson MDM, Ruppin E, Ronai ZA. Precision oncology: the road ahead. *Trends Mol Med*. 2017;23(10):874–898.
5. Joung JG, Oh BY, Hong HK, et al. Tumor heterogeneity predicts metastatic potential in colorectal cancer. *Clin Cancer Res*. 2017;23(23):7209–7216.
6. Ravasio R, Ceccacci E, Minucci S. Self-renewal of tumor cells: epigenetic determinants of the cancer stem cell phenotype. *Curr Opin Genet Dev*. 2016;36:92–99.
7. Batlle E, Clevers H. Cancer stem cells revisited. *Nat Med*. 2017;23(10):1124–1134.
8. García-Rubiño ME, Lozano-López C, Campos JM. Inhibitors of cancer stem cells. *Anticancer Agents Med Chem*. 2016;16(10):1230–1239.
9. Shibue T, Weinberg RA. EMT, CSCs, and drug resistance: the mechanistic link and clinical implications. *Nat Rev Clin Oncol*. 2017;14(10):611–629.
10. Gupta PB, Onder TT, Jiang G, et al. Identification of selective inhibitors of cancer stem cells by high-throughput screening. *Cell*. 2009;138(4):645–659.
11. Fu YZ, Yan YY, He M, et al. Salinomycin induces selective cytotoxicity to MCF-7 mammosphere cells through targeting the Hedgehog signaling pathway. *Oncol Rep*. 2016;35(2):912–922.
12. Dewangan J, Srivastava S, Rath SK. Salinomycin: A new paradigm in cancer therapy. *Tumour Biol*. 2017;39(3):1010428317695035.
13. Naujokat C, Steinhart R. Salinomycin as a drug for targeting human cancer stem cells. *J Biomed Biotechnol*. 2012;2012:950658–17.
14. Boehmerle W, Muenzfeld H, Springer A, Huehnchen P, Endres M. Specific targeting of neurotoxic side effects and pharmacological profile of the novel cancer stem cell drug salinomycin in mice. *J Mol Med*. 2014;92(8):889–900.
15. Milanovic M, Fan DNY, Belenki D, et al. Senescence-associated reprogramming promotes cancer stemness. *Nature*. 2018;553(7686):96–100.
16. Larzabal L, El-Nikhely N, Redrado M, et al. Differential effects of drugs targeting cancer stem cell (CSC) and non-CSC populations on lung primary tumors and metastasis. *PLoS One*. 2013;8(11):e79798.
17. Mao J, Song B, Shi Y, et al. ShRNA targeting Notch1 sensitizes breast cancer stem cell to paclitaxel. *Int J Biochem Cell Biol*. 2013;45(6):1064–1073.
18. Zhang Y, Zhang H, Wang X, et al. The eradication of breast cancer and cancer stem cells using octreotide modified paclitaxel active targeting micelles and salinomycin passive targeting micelles. *Biomaterials*. 2012;33(2):679–691.
19. Muntimadugu E, Kumar R, Saladi S, Rafeeqi TA, Khan W. CD44 targeted chemotherapy for co-eradication of breast cancer stem cells and cancer cells using polymeric nanoparticles of salinomycin and paclitaxel. *Colloids Surf B Biointerfaces*. 2016;143:532–546.
20. Kuo SZ, Blair KJ, Rahimy E, et al. Salinomycin induces cell death and differentiation in head and neck squamous cell carcinoma stem cells despite activation of epithelial-mesenchymal transition and Akt. *BMC Cancer*. 2012;12:556.
21. Maitz MF, Sperling C, Wongpinyochit T, et al. Biocompatibility assessment of silk nanoparticles: hemocompatibility and internalization by human blood cells. *Nanomedicine*. 2017;13(8):2633–2642.
22. Omenetto FG, Kaplan DL. New opportunities for an ancient material. *Science*. 2010;329(5991):528–531.
23. Raia NR, Partlow BP, McGill M, et al. Enzymatically crosslinked silk-hyaluronic acid hydrogels. *Biomaterials*. 2017;131:58–67.
24. Su D, Yao M, Liu J, et al. Enhancing mechanical properties of silk fibroin hydrogel through restricting the growth of β-sheet domains. *ACS Appl Mater Interfaces*. 2017;9(20):17489–17498.
25. Wang X, Kluge JA, Leisk GG, Kaplan DL. Sonication-induced gelation of silk fibroin for cell encapsulation. *Biomaterials*. 2008;29(8):1054–1064.
26. Zhang W, Wang X, Wang S, et al. The use of injectable sonication-induced silk hydrogel for $VEGF_{165}$ and BMP-2 delivery for elevation of the maxillary sinus floor. *Biomaterials*. 2011;32(35):9415–9424.
27. Seib FP, Pritchard EM, Kaplan DL. Self-assembling doxorubicin silk hydrogels for the focal treatment of primary breast cancer. *Adv Funct Mater*. 2013;23(1):58–65.
28. Numata K, Yamazaki S, Naga N. Biocompatible and biodegradable dual-drug release system based on silk hydrogel containing silk nanoparticles. *Biomacromolecules*. 2012;13(5):1383–1389.
29. Wu P, Liu Q, Li R, et al. Facile preparation of paclitaxel loaded silk fibroin nanoparticles for enhanced antitumor efficacy by locoregional drug delivery. *ACS Appl Mater Interfaces*. 2013;5(23):12638–12645.
30. Bian X, Wu P, Sha H, et al. Anti-EGFR-iRGD recombinant protein conjugated silk fibroin nanoparticles for enhanced tumor targeting and antitumor efficiency. *Onco Targets Ther*. 2016;9:3153–3162.
31. Dusi G, Gamba V. Liquid chromatography with ultraviolet detection of lasalocid, monensin, salinomycin and narasin in poultry feeds using pre-column derivatization. *J Chromatogr A*. 1999;835(1–2):243–246.
32. Mishra L, Banker T, Murray J, et al. Liver stem cells and hepatocellular carcinoma. *Hepatology*. 2009;49(1):318–329.
33. Kim UJ, Park J, Li C, et al. Structure and properties of silk hydrogels. *Biomacromolecules*. 2004;5(3):786–792.
34. Matsumoto A, Chen J, Collette AL, et al. Mechanisms of silk fibroin sol-gel transitions. *J Phys Chem B*. 2006;110(43):21630–21638.
35. Yucel T, Cebe P, Kaplan DL. Vortex-induced injectable silk fibroin hydrogels. *Biophys J*. 2009;97(7):2044–2050.
36. Numata K, Katashima T, Sakai T. State of water, molecular structure, and cytotoxicity of silk hydrogels. *Biomacromolecules*. 2011;12(6):2137–2144.
37. Wu X, Hou J, Li M, et al. Sodium dodecyl sulfate-induced rapid gelation of silk fibroin. *Acta Biomater*. 2012;8(6):2185–2192.
38. Wu H, Liu S, Xiao L, et al. Injectable and pH-responsive silk nanofiber hydrogels for sustained anticancer drug delivery. *ACS Appl Mater Interfaces*. 2016;8(27):17118–17126.
39. Coburn J, Harris J, Zakharov AD, et al. Implantable chemotherapy-loaded silk protein materials for neuroblastoma treatment. *Int J Cancer*. 2017;140(3):726–735.
40. Tian Y, Jiang X, Chen X, Shao Z, Yang W. Doxorubicin-loaded magnetic silk fibroin nanoparticles for targeted therapy of multidrug-resistant cancer. *Adv Mater*. 2014;26(43):7393–7398.
41. Qu J, Liu Y, Yu Y, et al. Silk fibroin nanoparticles prepared by electrospray as controlled release carriers of cisplatin. *Mater Sci Eng C Mater Biol Appl*. 2014;44:166–174.
42. Li H, Tian J, Wu A, et al. Self-assembled silk fibroin nanoparticles loaded with binary drugs in the treatment of breast carcinoma. *Int J Nanomedicine*. 2016;11:4373–4380.
43. Xie M, Fan D, Chen Y, et al. An implantable and controlled drug-release silk fibroin nanofibrous matrix to advance the treatment of solid tumour cancers. *Biomaterials*. 2016;103:33–43.
44. Lerdchai K, Kitsongsermthon J, Ratanavaraporn J, Kanokpanont S, Damrongsakkul S. Thai silk fibroin/gelatin sponges for the dual controlled release of curcumin and docosahexaenoic acid for anticancer treatment. *J Pharm Sci*. 2016;105(1):221–230.
45. Guziewicz N, Best A, Perez-Ramirez B, Kaplan DL. Lyophilized silk fibroin hydrogels for the sustained local delivery of therapeutic monoclonal antibodies. *Biomaterials*. 2011;32(10):2642–2650.
46. Guziewicz NA, Massetti AJ, Perez-Ramirez BJ, Kaplan DL. Mechanisms of monoclonal antibody stabilization and release from silk biomaterials. *Biomaterials*. 2013;34(31):7766–7775.
47. van Neerven SM, Tieken M, Vermeulen L, Bijlsma MF. Bidirectional interconversion of stem and non-stem cancer cell populations: A reassessment of theoretical models for tumor heterogeneity. *Mol Cell Oncol*. 2016;3(2):e1098791.